Bone Reports 18 (2023) 101692

Contents lists available at ScienceDirect

Bone Reports

journal homepage: www.elsevier.com/locate/bonr

Developmental impairments of craniofacial bone and cartilage in transgenic mice expressing FGF10

Hirotaka Yoshioka [a,b,*,1], Kazuko Kagawa [b,c,1], Tomoko Minamizaki [b], Masashi Nakano [b,d], Jane E. Aubin [e], Katsuyuki Kozai [f], Kazuhiro Tsuga [c], Yuji Yoshiko [b,**]

[a] Department of Anatomy, School of Medicine, International University of Health and Welfare, Chiba, Japan
[b] Department of Calcified Tissue Biology, Graduate School of Biomedical and Health Sciences, Hiroshima University, Hiroshima, Japan
[c] Department of Advanced Prosthodontics, Graduate School of Biomedical and Health Sciences, Hiroshima University, Hiroshima, Japan
[d] Department of Pediatric Dentistry, Division of Oral Health and Development, Hiroshima University Hospital, Hiroshima, Japan
[e] Department of Molecular Genetics, University of Toronto, Toronto, Ontario, Canada
[f] Department of Pediatric Dentistry, Graduate School of Biomedical and Health Sciences, Hiroshima University, Hiroshima, Japan

ARTICLE INFO

Keywords:
FGF10
FGFR2
Craniofacial skeleton
Chondrogenesis

ABSTRACT

Mutations in a common extracellular domain of fibroblast growth factor receptor (FGFR)-2 isoforms (type IIIb and IIIc) cause craniosynostosis syndrome and chondrodysplasia syndrome. FGF10, a major ligand for FGFR2-IIIb and FGFR1-IIIb, is a key participant in the epithelial-mesenchymal interactions required for morphogenetic events. FGF10 also regulates preadipocyte differentiation and early chondrogenesis in vitro, suggesting that FGF10-FGFR signaling may be involved in craniofacial skeletogenesis in vivo. To test this hypothesis, we used a tet-on doxycycline-inducible transgenic mouse model (FGF10 Tg) to overexpress *Fgf10* from embryonic day 12.5. *Fgf10* expression was 73.3-fold higher in FGF10 Tg than in wild-type mice. FGF10 Tg mice exhibited craniofacial anomalies, such as a short rostrum and mandible, an underdeveloped (cleft) palate, and no tympanic ring. Opposite effects on chondrogenesis in different anatomical regions were seen, e.g., hyperplasia in the nasal septum and hypoplasia in the mandibular condyle. We found an alternative splicing variant of *Fgfr2-IIIb* with a predicted translation product lacking the transmembrane domain, and suggesting a soluble form of FGFR2-IIIb (sFGFR2-IIIb), differentially expressed in some of the craniofacial bones and cartilages. Thus, excessive FGF10 may perturb signal transduction of the FGF-FGFR, leading to craniofacial skeletal abnormalities in FGF10 Tg mice.

1. Introduction

Craniofacial development requires highly organized cell-to-cell communication, often involving secreted factors and their cognate receptors that play roles in spatiotemporally-controlled events (Leitch et al., 2020; Wilkie and Morriss-Kay, 2001). Fibroblast growth factor (FGF)/FGF receptor (FGFR) signaling is one such essential pathway in craniofacial development (Moosa and Wollnik, 2016; Wilkie and Morriss-Kay, 2001). Members of the FGF family can be grouped into seven subfamilies, based on such criteria as sequence similarity and evolutionary relationships (Ornitz and Itoh, 2015). FGFs can act as intracrine, paracrine and endocrine factors via binding to a variety of FGFR family members, which signal through four different pathways: the JAK/STAT, Ras/MAPK, PI3K/Akt and PKC pathways (Ornitz and Itoh, 2015; Ornitz and Marie, 2015; Su et al., 2014).

FGFRs are encoded by four distinct genes (*Fgfr1–4*), and their transcripts are composed of two or three extracellular immunoglobulin (Ig)-like loops, a single transmembrane domain and two cytoplasmic tyrosine kinase domains (Ornitz and Itoh, 2015). Alternative splicing of exons encoding the third Ig-like loops in *Fgfr1–3* generate IIIb and IIIc

* Correspondence to: H. Yoshioka, Department of Anatomy, School of Medicine, International University of Health and Welfare, 4-3 Kozunomori, Narita, Chiba 286-8686, Japan.
** Correspondence to: Y. Yoshiko, Department of Calcified Tissue Biology, Graduate School of Biomedical and Health Sciences, Hiroshima University, 1-2-3 Kasumi, Minamiku, Hiroshima 734-8553, Japan.
E-mail addresses: yoshioka@iuhw.ac.jp (H. Yoshioka), yskyuji@yahoo.co.jp (Y. Yoshiko).
[1] These authors are contributed equally to this work.

https://doi.org/10.1016/j.bonr.2023.101692
Received 13 February 2023; Received in revised form 15 May 2023; Accepted 24 May 2023
Available online 26 May 2023

isoforms (Ornitz and Itoh, 2015). Mutations of FGFRs alter ligand-binding specificity and affinity, and, in some cases, constitutively activate receptor tyrosine kinases in a ligand-independent manner. These mutations are present in the common extracellular domain of FGFRs and are responsible for chondrodysplasia and craniosynostosis in congenital syndromes such as Apert syndrome, Crouzon syndrome and Pfeiffer syndrome (Ornitz and Itoh, 2015; Wilkie and Morriss-Kay, 2001).

Of 22 FGF family members, FGF10 binds to FGFR2-IIIb and other FGFRs including FGFR1-IIIb with high and low affinity, respectively (Zhang et al., 2006). Both *Fgf10* and *Fgfr2-IIIb* knockout mice are viable until birth and show similar deformities of multiple tissues requiring epithelial-mesenchymal interactions for development including the lung, salivary gland, palate and limb bud, with complete truncation of the fore- and hindlimbs (De Moerlooze et al., 2000; Hajihosseini et al., 2009; Rice et al., 2004; Sekine et al., 1999). The functional significance of FGF10 in rodent and human mesenchymal cells in vitro has also been reported. For example, neutralizing antibodies against FGF10 inhibited proliferation and adipogenic differentiation of mouse 3T3-L1 cells in association with a reduction of C/EBPα levels (Sakaue et al., 2002). Conflicting evidence exists on FGF10 activities in skeletogenic cells. For example, FGF10 was reported not to affect proliferation or differentiation of primary mouse calvaria osteoblastic cells, rib cage chondrocyte differentiation or osteoclast formation in mouse bone marrow cells cocultured with osteoblasts (Shimoaka et al., 2002). FGF10 inhibited cell proliferation in human growth plate chondrocyte cultures (Olney et al., 2004), while overexpression of *Fgf10* in organ cultures and micromass cell cultures of fetal rat mandibular processes enhanced chondrogenic differentiation (Terao et al., 2011). Taken together, these results raise the possibility that FGF10 may directly target bone and cartilage, but the role of FGF10 in osteo/chondrogenic cells in vivo remains to be clarified. To address this issue, we prepared transgenic mice overexpressing *Fgf10* and analyzed in detail the pronounced effects of excess FGF10 on development of the craniofacial skeleton.

2. Materials and methods

2.1. Transgenic mice overexpressing Fgf10 (FGF10 Tg mice)

Transgenic mice constitutively expressing *CMV-rtTA* (Parsa et al., 2010) and *tet(o)Fgf10* (Clark et al., 2001) were provided by the Jackson Laboratory (Bar Harbor, ME) and by Dr. Jeffrey A. Whitsett (Cincinnati Children's Hospital Medical Center, OH), respectively. All mice were conventionally reared and fed with a regular diet. Mice were genotyped as described (http://www.jax.org/index.html). To obtain fetuses ubiquitously overexpressing *Fgf10* (*CMV-rtTA*$^{tg/+}$;*tet(o)Fgf10*$^{tg/tg}$ and/or *CMV-rtTA*$^{tg/+}$; *tet(o)Fgf10* $^{tg/+}$) and control fetuses (*tet(o)Fgf10*$^{tg/tg}$ and/or *tet(o)Fgf10*$^{tg/+}$) as littermates, female mice (*tet(o)Fgf10*$^{tg/tg}$) were bred with male mice (*CMV-rtTA*$^{tg/+}$;*tet(o)Fgf10*$^{tg/+}$). The day of vaginal plug detection was defined as embryonic day (E) 0.5. *Fgf10* expression was induced in pregnant mice by ad libitum water containing 2 mg/mL of doxycycline hyclate (Dox; Sigma-Aldrich, St Louis, MO) in 5 % sucrose from E12.5. Note that Dox in drinking water is delivered to organs within 4 h and reaches a maximum after 24 h (Kistner et al., 1996) and that pregnant mice were not affected by Dox (Fedorov et al., 2001). Five animals were used in each group. Animal use and procedures were approved by the Committee of Animal Experimentation at Hiroshima University (#A15–142).

2.2. Microcomputed tomography (μCT) analysis

Neonates were analyzed using μCT (Skyscan 1176; Bruker, Billerica, MA) under the following conditions: voltage 40 kV, current 600 μA, image pixel size 17.5 μm, and no filter. Images were reconstructed using NRecon (Bruker).

2.3. Whole-mount skeletal staining

Whole-mount skeletal staining was performed as described previously (Kimmel and Trammell, 1981). Briefly, neonates were skinned and eviscerated, and stained with 0.14 % Alcian blue and 0.12 % Alizarin red S in ethanol and glacial acetic acid. Specimens were then cleared in 2 % potassium hydroxide and stored in 50 % (vol/vol) glycerin.

2.4. Paraffin sections and histology

Fetuses at E18.5 were fixed in 4 % paraformaldehyde in PBS at 4 °C overnight and demineralized in 10 % EDTA in PBS at 4 °C for a few days, followed by dehydration and paraffin embedding. Deparaffinized sections (5 μm thickness) were stained with hematoxylin and eosin (HE). For immunohistochemistry, sections were pretreated with 0.1 % hyaluronidase in TBS (20 mM Tris-HCl, 150 mM NaCl, pH 7.6) at 37 °C for 60 min, followed by Protein Block (DAKO, Glostrup, Denmark) for 30 min at room temperature. Sections were then incubated with primary antibodies against type X collagen (1:1000; Cosmo Bio, Tokyo, Japan) at 4 °C overnight. Alexa Fluor 594 goat anti-rabbit IgG (1:500; Life Technologies, Carlsbad, CA) was used as a secondary antibody, and sections were mounted in Vectashield with DAPI (Vector Laboratories, Burlingame, CA). Normal rabbit IgG was used as a negative control.

2.5. RT-PCR and sequence analysis

Mandibular condylar cartilages were isolated from E18.5 fetuses (Control, $n = 8$–13; FGF10 Tg, $n = 7$–15) carried by 2–3 pregnant mice in each experiment and pooled for RNA isolation. Tissues were collected form wild-type neonate mice for RNA isolation. Total RNA was isolated using TriPure Isolation Reagent (Roche Diagnostics, Indianapolis, IN) and reverse transcribed using ReverTraAce, according to the manufacturer's instructions (Toyobo, Osaka, Japan). Gene expression was quantified by real-time PCR (StepOnePlus real-time PCR system, Life Technologies) using Fast SYBR Green Master Mix (Life Technologies). PCR was performed with KOD Fx Neo polymerase (Toyobo). Primers used are as follows: *Fgf10*, 5′-AGC GGG ACC AAG AAT GAA G-3′, 5′-GCT GTT GAT GGC TTT GAC G-3′; *Sox9*, 5′-CTA TCT TCA AGG CGC TGC AA-3′, 5′-GTC GGT TTT GGG AGT GGT G-3′; *H4c*, 5′-CGG TGT GCT GAA GGT GTT CC-3′, 5′-ACC GCC GAA TCC GTA GAG AG-3′; *Runx2*, 5′-TTC TGC CTC TGG CCT TCC TC-3′, 5′-AAG GGC CCA GTT CTG AAG CA-3′; *Col2a1*, 5′-GTG GAG CAG CAA GAG CAA GG-3′, 5′-CTG GAC GTT AGC GGT GTT GG-3′; *Col10a1*, 5′-GGC AGA GGA AGC CAG GAA AG-3′, 5′-TTA GCA GCA GAA AGG GTA TTT GAG G-3′; *Fgfr2-IIIb*, 5′-CTC ACT GTC CTG CCC AAA CA-3′, 5′-CAC CAT GCA GGC GAT TAA GA-3′; *Fgfr2-IIIc*, 5′-GCT TCA TCT GCC TGG TCT TGG-3′, 5′-TGG GAG ATT TGG TAT TTG GTT GG-3′; *Actb*, 5′-GGC TGT ATT CCC CTC CAT CG-3′, 5′-GCC TCG TCA CCC ACA TAG GA-3′ (forward and reverse, respectively). *Actb* was used as an internal control. PCR products were analyzed by electrophoresis in a 2 % agarose gel and stained with ethidium bromide (Wako Pure Chemical Industries, Osaka, Japan). PCR products of *Fgfr2-IIIb* were cloned into pcDNA3.1 vector and sequenced by Eurofins Genomics (Tokyo, Japan). The obtained sequence was analyzed in the GenBank database using NCBI BLAST search tools (https://blast.ncbi.nlm.nih.gov/Blast.cgi).

2.6. Statistical analysis

Data are expressed as mean ± SD. Non-numerical data are shown as representative results of three independent experiments. Statistical differences were evaluated using F-test followed by Student's or Welch's *t*-test. A p-value <0.05 was considered statistically significant.

3. Results

3.1. Craniofacial skeletal anomalies in FGF10 Tg mice

In keeping with the observation that early skeletogenesis in mice is seen in limbs at E11.5–13.5 (Kaufman, 1992) and in the craniofacial complex (chondrocranium) at E11 (McBratney-Owen et al., 2008), we induced *Fgf10* expression from E12.5. FGF10 Tg mice were viable until birth but died soon after. Amongst the substantial anomalies detected by whole-mount skeletal staining of FGF10 Tg neonates, significant craniofacial shape abnormalities were seen, such as a shorter rostrum and mandible compared to control (Fig. 1A, B). FGF10 Tg mice also exhibited defects in cranial bones and sutures, especially coronal, sagittal, and lambdoid sutures (Fig. 1B, C). Overexpression of *Fgf10* also caused cleft palate and tympanic ring defects (Fig. 1D). Cartilage dysplasia was observed especially in the frontonasal cartilage, mandibular condylar cartilage, mandibular angular cartilage and the rostral process of Meckel's cartilage (Fig. 1C–E). Skeletal anomalies were not restricted to the craniofacial complex; for example, mineralized phalanges were absent (Fig. 1B). On the other hand, whole-mount staining revealed no obvious cartilage-bone defects in the limbs or vertebrae of FGF10 Tg mice, although limb bones appeared to be shorter. Results of μCT analyses largely mirrored the results of whole-mount skeletal staining and demonstrated in more detail the craniofacial bone dysmorphologies including of the parietal bone, interparietal bone, supraoccipital bone, and exoccipital bone (Fig. 2A). Quantification confirmed the significantly smaller cranial size and mandibular length and the larger palatal width in the temporal region (Fig. 2B) as well as the shortened limb bones (Fig. 2C) in FGF10 Tg versus control mice. We focused the rest of our analyses on the craniofacial complex.

3.2. Histological and gene expression analyses of craniofacial skeletal anomalies in FGF10 Tg mice

HE staining was performed to assess histological changes in craniofacial skeleton of FGF10 Tg compared to littermate control mice (Fig. 3A, I). *Fgf10* overexpression induced marked anomalies of epithelial cells, with lack of keratinization (Fig. 3B, J), invagination of epithelial cells into connective tissue (Fig. 3C, K), and hyperplasia of exocrine glands (Fig. 3D, L). Hyperplasia of adipose tissue was also evident (Fig. 3E, M). In contrast to the hypoplasia seen in the mandibular condylar cartilage (Fig. 1), hyperplasia of cartilage in the nasal septum, nasal concha, and cranial base was observed in FGF10 Tg neonates (Fig. 3F–H, N–P).

Immunostaining of type X collagen, a marker of hypertrophic chondrocytes, demonstrated a reduction of the hypertrophic zone in

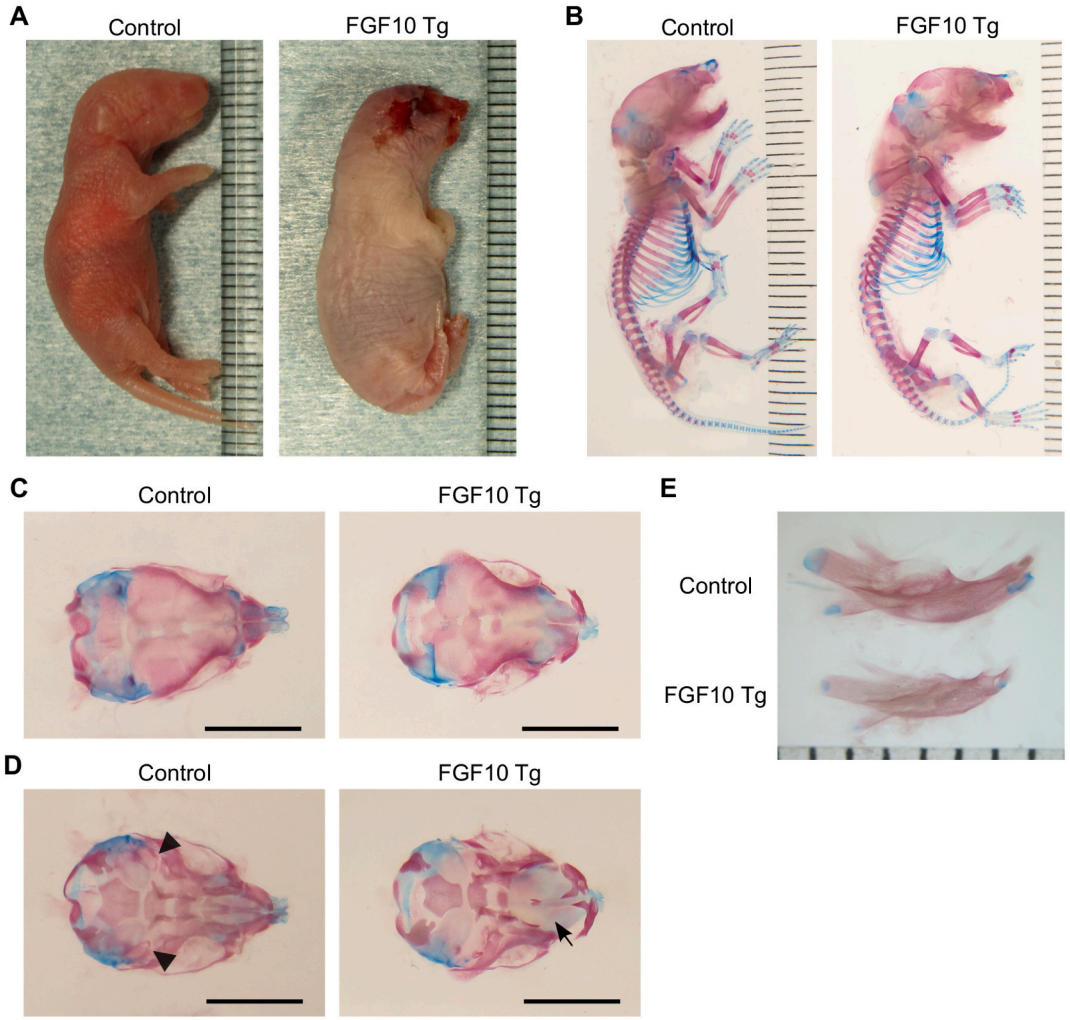

Fig. 1. Skeletal anomalies in FGF10 Tg mice. (A) Gross appearance of neonate mice. (B–E) Skeletons of neonates stained with Alizarin red and Alcian blue. Superior (C) and inferior (D) views of craniofacial skeletons and lateral view of mandibles (E). Mandibles were removed to show inferior view of the cranial base (D). Tympanic rings (arrowheads) were observed in control but not FGF10 Tg mice. Cleft palate (arrow) in FGF10 Tg mice. Rulers are in millimeters (A, B, E). Scale bars, 5 mm (C, D).

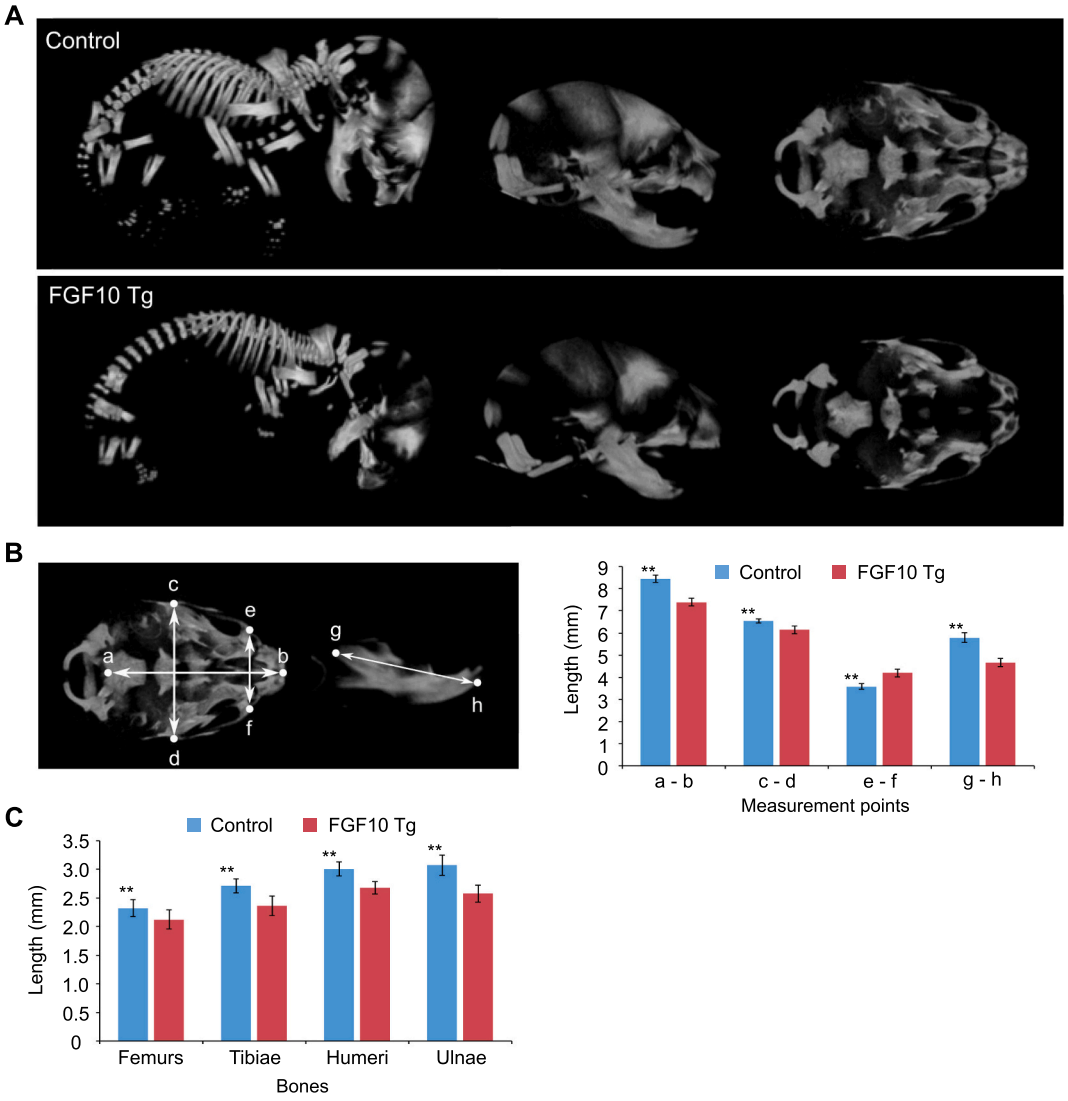

Fig. 2. μCT analysis of craniofacial skeletons. (A) Three-dimensional reconstructions from μCT images of control and FGF10 Tg neonates. Whole skeletons (left), and lateral (middle) and inferior (right) views of craniofacial skeletons are shown. Mandibles were removed to show inferior view of the cranial base. (B) Morphological evaluation of the craniofacial skeletons. The landmarks (a–h) shown in the left column were used for the axial length measurements shown in the right column. (C) Morphological evaluation of long bones. Error bars indicate SEM. $n = 10$. **, $p < 0.01$.

mandibular condylar cartilage in FGF10 Tg compared to control mice (Fig. 4A–D). To characterize the molecular basis of the hypoplasia, we compared expression levels of *Fgf10* and osteochondrogenesis-related genes between control and FGF10 Tg mandibular condylar cartilage. *Fgf10* expression was 73.3-fold higher (average of 3 experiments) in FGF10 Tg compared to control specimens (Fig. 4E), while amongst the osteochondrogenesis-related genes analyzed, *Runx2* was increased and *Col10a1* was decreased (Fig. 4F). Taken together with the result that no difference was seen in the expression of *H4c*, a proliferation marker, these results suggest that an excess of *Fgf10* may inhibit the terminal differentiation of chondrocytes, resulting in cartilage and bone hypoplasia.

3.3. *Expression profiles of Fgf10 and receptors Fgfr2-IIIb and Fgfr2-IIIc in mouse tissues*

To explore the mechanism underlying the regulation of osteochondrogenesis by FGF10 signaling, we analyzed the expression profiles of the *Fgf10*, *Fgfr2-IIIb*, and *Fgfr2-IIIc* genes by RT-PCR in multiple tissues of wild-type neonatal mice and the prechondrogenic mouse cell line ATDC5 (Fig. 5A). Most of the tissues analyzed as well as the ATDC5 cells expressed all three transcripts, but an unexpected longer RT-PCR product of *Fgfr2-IIIb* was identified in both ATDC5 cells and in the cartilages and bones exhibiting dysplasia in FGF10 Tg mice (Figs. 1, 2). Sequencing of the longer RT-PCR product identified sequences corresponding to exon 8 and 9, encoding IIIb and IIIc respectively (Fig. 5B), and sharing high sequence similarity (99.62 %) with an alternative splicing variant of *Fgfr2* (GenBank accession number EF143332, from nucleotides 796 to 1057). The inclusion of exon 9 in *Fgfr2-IIIb* mRNA may result in a frameshift and subsequent premature stop codon soon after the immunoglobulin (Ig)-like domain III (Fig. 5B, C). Consequently, a truncated form of FGFR2-IIIb lacking the transmembrane and tyrosine kinase domains may be produced and secreted as a soluble form (sFGFR2-IIIb) (Fig. 5C).

4. Discussion

We report here that high (~73-fold) overexpression of *Fgf10* in mouse fetuses induced developmental anomalies in craniofacial cartilage and bone. The consequences of *Fgf10* overexpression on differentiation of various lineages and the associated signaling factor regulatory pathways is known to be complex. For example, modest overexpression

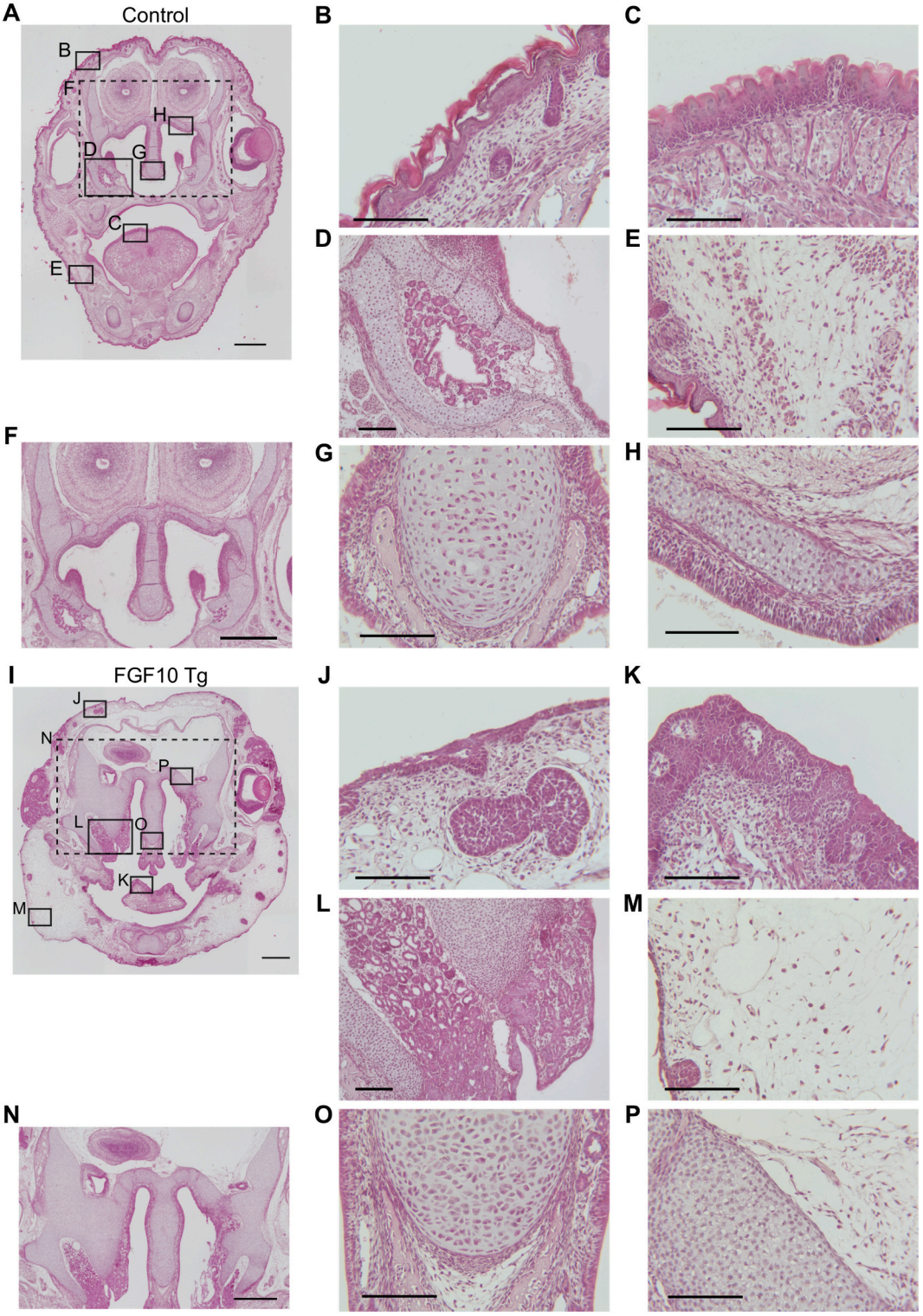

Fig. 3. Histology of craniofacial skeletons. Coronal sections of control (A–H) and FGF10 Tg (I-P) fetuses were stained with HE. Higher magnifications of areas enclosed by solid lines in (A) and (I) are indicated in (B–E, G, H) and (J–M, O, P), respectively. The skin (B, J), tongue (C, K), nasal gland (D, L), and adipose tissue (E, M) are shown. Areas enclosed by dashed lines in (A) and (I) correspond to (F) and (N), respectively. Cartilages around the nasal septum (G, O), nasal concha, and cranial base (H, P) are shown (F, N). Scale bars, 500 μm (A, F, I, N); 100 μm (B–E, G, H, J–M, O, P).

of *Fgf10* (2- to 4-fold) under the control of the *Ipf1* promoter maintained Notch signaling activation throughout the pancreatic epithelium, leading to the impaired differentiation of pancreatic cells (Hart et al., 2003). On the other hand, somewhat higher overexpression of *Fgf10* (11-fold) attenuated bleomycin-induced lung fibrosis at least in part via a reduction in TGF-β expression and activity (Gupte et al., 2009). Some or all of the skeletal anomalies we observe with high overexpression of *Fgf10* in our Tg mice may result in changes of expression and/or activities of other signaling factors also involved in skeletal development (see below) or may result, at least in part, from the high overexpression

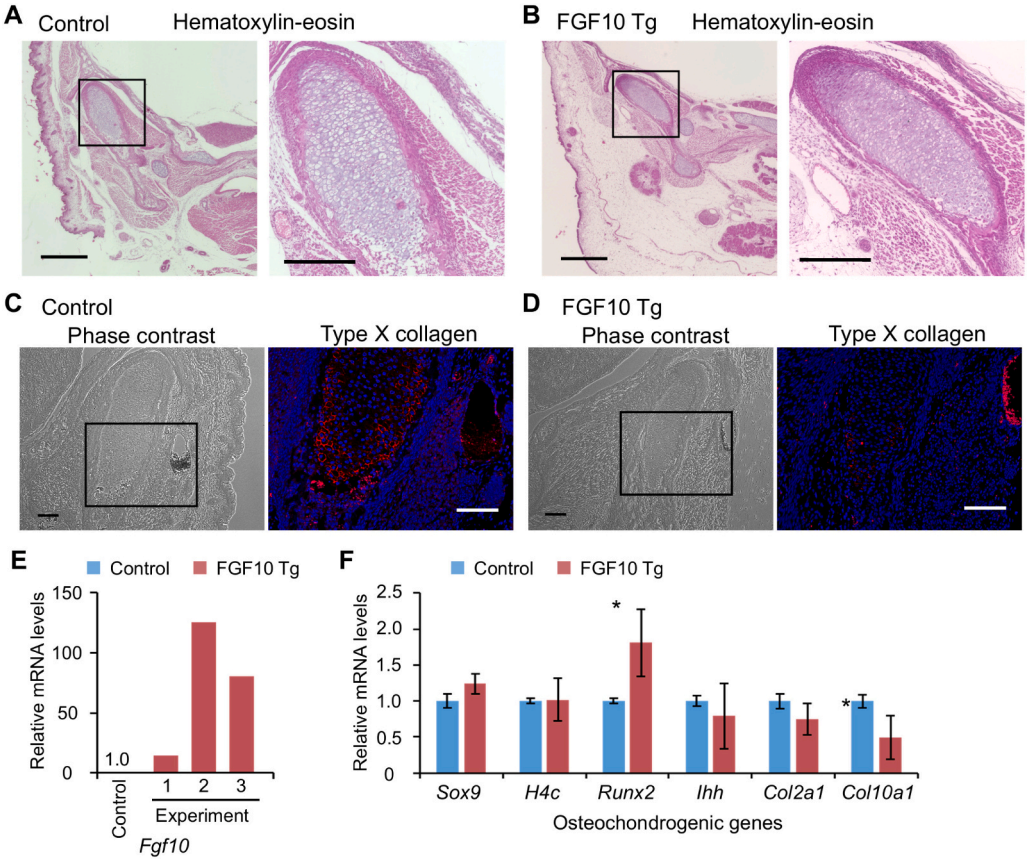

Fig. 4. Histological and gene expression analyses of the mandibular condylar cartilage. Coronal sections of the condylar cartilage in control (A, C) and FGF10 Tg (B, D) fetuses were stained with HE (A, B) and antibodies against type X collagen (C, D). Higher magnifications of areas enclosed by solid lines in left panels are shown in the right panels (A, B). Areas enclosed by solid lines (phase contrast) correspond to type X collagen (red) immunohistochemistry (C, D). DAPI (blue) was used for nuclear staining. Scale bars, 500 μm (left in A and B); 200 μm (right in A and B); 100 μm (C, D). Levels of *Fgf10* (E) and osteochondrogenic genes (F) in the mandibular condylar cartilage of control and FGF10 Tg mice. Relative mRNA levels in the control are set at 1. For *Fgf10* gene, three independent experiments are shown. For osteochondrogenic genes, error bars indicate SD. $n = 3$. *, $p < 0.05$.

overwhelming the FGF signaling pathway itself, issues that require additional studies.

Actions of FGF10 appear to be mediated primarily by communication between FGF10-producing mesenchymal cells and specific FGFR-expressing epithelial cells (Ornitz and Itoh, 2015), resulting in FGF10-induced increases in epithelial cell proliferation (Igarashi et al., 1998; Marchese et al., 2001). This mitogenic effect of FGF10 on epithelial cells may have caused lung dysplasia in our Tg mice, leading to their death soon after birth, as is the case in mouse fetuses infected with FGF10 adenoviruses (Gonzaga et al., 2008). We also infer that the excess *Fgf10* in our Tg mice accelerates proliferation and impedes differentiation of epithelial cells, leading to a defective cornified layer and hyperplasia of glands (Fig. 3J–L). The hyperplasia of adipose tissues (Fig. 3M) in the FGF10 Tg mice is also consistent with the observation that FGF10 coordinates the proliferation and differentiation of adipocytes by activating CEBP/α and PPARγ (Ohta and Itoh, 2014; Sakaue et al., 2002).

Our results are consistent with the view that overexpression of *Fgf10* reduced chondrocyte hypertrophy in mandibular condylar cartilage (Fig. 4A–D) as a consequence of increased expression of *Runx2*, a transcription factor required for chondrocyte differentiation (Fig. 4F). Although knockout and transgenic mouse studies have shown that *Runx2* expressed in prehypertrophic chondrocytes triggers hypertrophy of chondrocytes by activating *Ihh* and *Col10a1* (Yoshida et al., 2004; Zheng et al., 2003), loss- and gain-of-function mouse models have also shown that the long-lasting expression of *Runx2* in perichondrocytes inhibits chondrocyte proliferation and hypertrophy (Hinoi et al., 2006). FGF10 Tg mice also showed thickening of the cartilage in the nasal septum, nasal concha, and cranial base (Fig. 3). These phenotypic anomalies are also observed in the $Fgfr2^{C342Y}$ Crouzon syndrome mouse model (Perrine et al., 2022), while the $Fgfr2^{S252W}$ Apert syndrome mouse model shows no cartilage abnormalities in the cranial base (Kim et al., 2020). Despite activating the same receptor, different mutations in *Fgfr2* give rise to different effects even at very close sites such as the nasal septum and cranial base, paralleling the differential effects that we see in FGF10 Tg mice which exhibit hypoplasia in mandibular condylar cartilage but hyperplasia of cartilage in the closely positioned nasal septum and cranial base. These diverse effects at different albeit closely positioned sites may reflect the fact that cartilages of the chondrocranium form individually, appearing at different points of embryonic time and maturing according to their own developmental schedule (see Perrine et al., 2022 for detailed discussion). Such developmental differences suggest that FGF10 could affect the chondrocytes of different sites based on developmental time-dependent changes in other regulatory molecules in the environment and/or in specific cells of different cartilage zones (e.g., proliferative versus hypertrophic), such as *Runx2*, as mentioned above and/or the potential alternatively spliced variant of *Fgfr2-IIIb* that we have identified in some bones and cartilages (see below). Further studies will be necessary to dissect the mechanisms underlying the aberrant chondrogenesis in the FGF10 Tg mice.

Mutations in the FGF signaling pathway are the most common cause of craniosynostosis, characterized by the premature fusion of cranial sutures (Ornitz and Itoh, 2015; Wilkie and Morriss-Kay, 2001). However, FGF10 Tg mice exhibited the opposite phenotype, with wider sutures (Fig. 1C, 2A). This suggests that excess FGF10 affects not only endochondral ossification but also intramembranous ossification. Intramembranous ossification is known to be regulated by several signaling pathways, including FGFs (Ornitz and Marie, 2015), as exemplified for example by the severe defects in cranial bones seen in double knockout mice lacking *Fgf9* and *Fgf18* (Hung et al., 2016). Amongst possible mechanisms when FGF is in excess is the induction of SOX2, which has been shown to result in the inhibition of osteoblast differentiation and parietal bone hypoplasia (Holmes et al., 2011), consistent with the hypoplastic cranial bones with enlarged cranial sutures seen in our Tg mice. We also cannot discount possible indirect

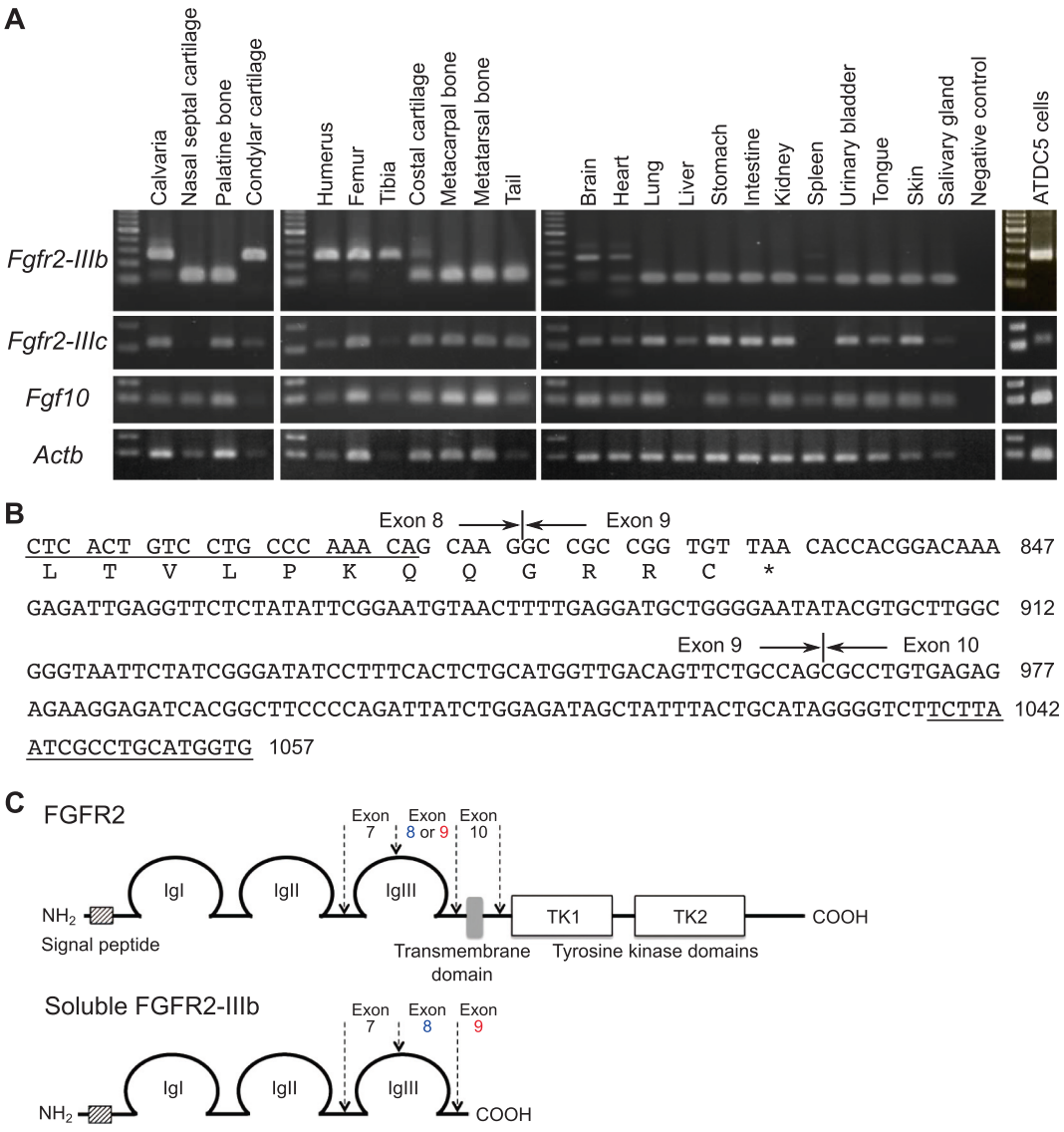

Fig. 5. (A) Expression profiles of *Fgfr2* and *Fgf10* genes in wild-type mouse tissues and the prechondrogenic cell line ATDC5; the ß-actin gene (*Actb*) was used as internal control. (B) cDNA sequence and deduced amino acid sequence of *Fgfr2*. Asterisk shows stop codon. PCR primers used are indicated by underlined letters. The numbers on the right indicate the nucleotide positions corresponding to the GenBank accession number EF143332. (C) Schematic structures of FGFR2 and soluble FGFR2-IIIb (sFGFR2-IIIb).

effects on osteoblast lineage cells of FGF10 excess via other non-osteoblast lineage cells in the developing chondrocranium and dermal cranium tissue complex. Elucidating potential osteoblast lineage autonomous versus nonautonomous mechanisms of FGF10 on cranial sutures will be addressed in future.

We identified a potential alternative splicing variant of *Fgfr2-IIIb* in some bones and cartilages of wild-type mice (Fig. 5). This variant, sFGFR2-IIIb, may act as a decoy receptor for FGF10 and/or other FGF subfamilies including FGF3, FGF7, and FGF22 to modulate its (their) signal transduction. Considering the fact that human FGFR2 forms heterodimers with human FGFR1 in vitro (Wang et al., 1997), heterodimerization of sFGFR2-IIIb and FGFR1 could also participate in the FGF signaling pathway. Thus, it is notable that the cartilages and bones where *sFgfr2-IIIb* was expressed (no expression of membranous type *Fgfr2-IIIb*) were those exhibiting hypoplasia in the FGF10 Tg mice. An excess of FGF10 may trap sFGFR2-IIIb and allow extraordinary FGF signaling by the remainder and/or other FGFs. For example, a surplus of FGF10 may bind to FGFR1 involved in the terminal maturation of mouse hypertrophic chondrocytes (Jacob et al., 2006). Indeed, constitutive FGFR1 activity causes osteoglophonic dysplasia, characterized by multiple osteochondrogenic anomalies such as rhizomelic dwarfism, craniosynostosis, and low bone mineral density (White et al., 2005). On the other hand, we found that cartilages and bones expressing the membranous *Fgfr2-IIIb* showed either hyperplasia or no phenotypes (Figs. 1, 2, 5A). FGF10 is a key factor for epithelial-mesenchymal interaction and induces the expression of ectodermal FGF8 (Itoh, 2016) that promotes chondrogenesis during chick cranial development (Abzhanov and Tabin, 2004). Thus, sFGFR2-IIIb scavenging by an excess of FGF10 may elicit abundant FGF8 that may accelerate the growth of cartilage in the nasal septum, nasal concha, and cranial base of FGF10 Tg mice (Fig. 3).

In conclusion, we made the unexpected observation of diverse site-specific dysmorphologies in development of the craniofacial skeletal in FGF10 Tg mice and site-specific expression of an alternative splicing variant of *Fgfr2-IIIb*, *sFgfr2-IIIb*. Further studies are necessary to dissect the regulatory mechanisms underlying these diverse effects of over-expression of FGF10 in relation to sFGFR2-IIIb.

CRediT authorship contribution statement

Hirotaka Yoshioka: Conceptualization, Formal analysis, Investigation, Methodology, Supervision, Visualization, Writing – review & editing. **Kazuko Kagawa:** Conceptualization, Formal analysis, Investigation, Methodology, Writing – original draft. **Tomoko Minamizaki:** Conceptualization, Investigation, Methodology. **Masashi Nakano:** Investigation. **Jane E. Aubin:** Supervision, Writing – review & editing. **Katsuyuki Kozai:** Supervision. **Kazuhiro Tsuga:** Supervision. **Yuji Yoshiko:** Conceptualization, Investigation, Methodology, Project administration, Supervision, Writing – review & editing.

Declaration of competing interest

The authors declare that there is no conflict of interest.

Data availability statement

The data that support the findings of this study are available from the corresponding authors upon reasonable request.

Acknowledgements

We thank Dr. Jeffrey A. Whitsett for providing the *tet(o)Fgf10* mice and Dr. Koh-ichi Kuremoto for his generous support. This work was supported by JSPS KAKENHI (#17K11804).

References

Abzhanov, A., Tabin, C.J., 2004. Shh and Fgf8 act synergistically to drive cartilage outgrowth during cranial development. Dev. Biol. 273, 134–148. https://doi.org/10.1016/j.ydbio.2004.05.028.

Clark, J.C., Tichelaar, J.W., Wert, S.E., Itoh, N., Perl, A.-K.T., Stahlman, M.T., Whitsett, J. A., 2001. FGF-10 disrupts lung morphogenesis and causes pulmonary adenomas in vivo. Am. J. Physiol. Lung Cell. Mol. Physiol. 280, L705–L715. https://doi.org/10.1152/ajplung.2001.280.4.L705.

De Moerlooze, L., Spencer-Dene, B., Revest, J.M., Hajihosseini, M., Rosewell, I., Dickson, C., 2000. An important role for the IIIb isoform of fibroblast growth factor receptor 2 (FGFR2) in mesenchymal-epithelial signalling during mouse organogenesis. Development 127, 483–492. https://doi.org/10.1242/dev.127.3.483.

Fedorov, L.M., Tyrsin, O.Y., Krenn, V., Chernigovskaya, E.V., Rapp, U.R., 2001. Tet-system for the regulation of gene expression during embryonic development. Transgenic Res. 10, 247–258. https://doi.org/10.1023/a:1016632110931.

Gonzaga, S., Henriques-Coelho, T., Davey, M., Zoltick, P.W., Leite-Moreira, A.F., Correia-Pinto, J., Flake, A.W., 2008. Cystic adenomatoid malformations are induced by localized FGF10 overexpression in fetal rat lung. Am. J. Respir. Cell Mol. Biol. 39, 346–355. https://doi.org/10.1165/rcmb.2007-0290OC.

Gupte, V.V., Ramasamy, S.K., Reddy, R., Lee, J., Weinreb, P.H., Violette, S.M., Guenther, A., Warburton, D., Driscoll, B., Minoo, P., Bellusci, S., 2009. Overexpression of fibroblast growth factor-10 during both inflammatory and fibrotic phases attenuates bleomycin-induced pulmonary fibrosis in mice. Am. J. Respir. Crit. Care Med. 180, 424–436. https://doi.org/10.1164/rccm.200811-1794OC.

Hajihosseini, M.K., Duarte, R., Pegrum, J., Donjacour, A., Lana-Elola, E., Rice, D.P., Sharpe, J., Dickson, C., 2009. Evidence that Fgf10 contributes to the skeletal and visceral defects of an Apert syndrome mouse model. Dev. Dyn. 238, 376–385. https://doi.org/10.1002/dvdy.21648.

Hart, A., Papadopoulou, S., Edlund, H., 2003. Fgf10 maintains notch activation, stimulates proliferation, and blocks differentiation of pancreatic epithelial cells. Dev. Dyn. 228, 185–193. https://doi.org/10.1002/dvdy.10368.

Hinoi, E., Bialek, P., Chen, Y.-T., Rached, M.-T., Groner, Y., Behringer, R.R., Ornitz, D.M., Karsenty, G., 2006. Runx2 inhibits chondrocyte proliferation and hypertrophy through its expression in the perichondrium. Genes Dev. 20, 2937–2942. https://doi.org/10.1101/gad.1482906.

Holmes, G., Bromage, T.G., Basilico, C., 2011. The Sox2 high mobility group transcription factor inhibits mature osteoblast function in transgenic mice. Bone 49, 653–661. https://doi.org/10.1016/j.bone.2011.06.008.

Hung, I.H., Schoenwolf, G.C., Lewandoski, M., Ornitz, D.M., 2016. A combined series of Fgf9 and Fgf18 mutant alleles identifies unique and redundant roles in skeletal development. Dev. Biol. 411, 72–84. https://doi.org/10.1016/j.ydbio.2016.01.008.

Igarashi, M., Finch, P.W., Aaronson, S.A., 1998. Characterization of recombinant human fibroblast growth factor (FGF)-10 reveals functional similarities with keratinocyte growth factor (FGF-7). J. Biol. Chem. 273, 13230–13235. https://doi.org/10.1074/jbc.273.21.13230.

Itoh, N., 2016. FGF10: a multifunctional mesenchymal–epithelial signaling growth factor in development, health, and disease. Cytokine Growth Factor Rev. 28, 63–69. https://doi.org/10.1016/j.cytogfr.2015.10.001.

Jacob, A.L., Smith, C., Partanen, J., Ornitz, D.M., 2006. Fibroblast growth factor receptor 1 signaling in the osteo-chondrogenic cell lineage regulates sequential steps of osteoblast maturation. Dev. Biol. 296, 315–328. https://doi.org/10.1016/j.ydbio.2006.05.031.

Kaufman, M., 1992. The Atlas of Mouse Development. Academic Press.

Kim, B., Shin, H., Kim, W., Kim, H., Cho, Y., Yoon, H., Baek, J., Woo, K., Lee, Y., Ryoo, H., 2020. PIN1 attenuation improves midface hypoplasia in a mouse model of Apert syndrome. J. Dent. Res. 99, 223–232. https://doi.org/10.1177/0022034519893656.

Kimmel, C.A., Trammell, C., 1981. A rapid procedure for routine double staining of cartilage and bone in fetal and adult animals. Stain. Technol. 56, 271–273. https://doi.org/10.3109/10520298109067325.

Kistner, A., Gossen, M., Zimmermann, F., Jerecic, J., Ullmer, C., Lubbert, H., Bujard, H., 1996. Doxycycline-mediated quantitative and tissue-specific control of gene expression in transgenic mice. Proc. Natl. Acad. Sci. U. S. A. 93, 10933–10938. https://doi.org/10.1073/pnas.93.20.10933.

Leitch, V.D., Bassett, J.H.D., Williams, G.R., 2020. Role of thyroid hormones in craniofacial development. Nat. Rev. Endocrinol. 16, 147–164. https://doi.org/10.1038/s41574-019-0304-5.

Marchese, C., Felici, A., Visco, V., Lucania, G., Igarashi, M., Picardo, M., Frati, L., Torrisi, M.R., 2001. Fibroblast growth factor 10 induces proliferation and differentiation of human primary cultured keratinocytes. J. Invest. Dermatol. 116, 623–628. https://doi.org/10.1046/j.0022-202x.2001.01280.x.

McBratney-Owen, B., Iseki, S., Bamforth, S.D., Olsen, B.R., Morriss-Kay, G.M., 2008. Development and tissue origins of the mammalian cranial base. Dev. Biol. 322, 121–132. https://doi.org/10.1016/j.ydbio.2008.07.016.

Moosa, S., Wollnik, B., 2016. Altered FGF signalling in congenital craniofacial and skeletal disorders. Semin. Cell Dev. Biol. 53, 115–125. https://doi.org/10.1016/j.semcdb.2015.12.005.

Ohta, H., Itoh, N., 2014. Roles of FGFs as adipokines in adipose tissue development, remodeling, and metabolism. Front. Endocrinol. 5, 18. https://doi.org/10.3389/fendo.2014.00018.

Olney, R.C., Wang, J., Sylvester, J.E., Mougey, E.B., 2004. Growth factor regulation of human growth plate chondrocyte proliferation in vitro. Biochem. Biophys. Res. Commun. 317, 1171–1182. https://doi.org/10.1016/j.bbrc.2004.03.170.

Ornitz, D.M., Itoh, N., 2015. The fibroblast growth factor signaling pathway. Dev. Biol. 4, 215–266. https://doi.org/10.1002/wdev.176.

Ornitz, D.M., Marie, P.J., 2015. Fibroblast growth factor signaling in skeletal development and disease. Genes Dev. 29, 1463–1486. https://doi.org/10.1101/gad.266551.115.

Parsa, S., Kuremoto, K., Seidel, K., Tabatabai, R., MacKenzie, B., Yamaza, T., Akiyama, K., Branch, J., Koh, C.J., Alam, D.A., Klein, O.D., Bellusci, S., 2010. Signaling by FGFR2b controls the regenerative capacity of adult mouse incisors. Development 137, 3743–3752. https://doi.org/10.1242/dev.051672.

Perrine, S.M.M., Pitirri, M.K., Durham, E.L., Kawasaki, M., Zheng, H., Chen, D.Z., Kawasaki, K., Richtsmeier, J.T., 2022. A dysmorphic mouse model reveals developmental interactions of chondrocranium and dermatocranium. eLife 11, e76653. https://doi.org/10.7554/eLife.76653.

Rice, R., Spencer-Dene, B., Connor, E.C., Gritli-Linde, A., McMahon, A.P., Dickson, C., Thesleff, I., Rice, D.P.C., 2004. Disruption of Fgf10/Fgfr2b-coordinated epithelial-mesenchymal interactions causes cleft palate. J. Clin. Invest. 113, 1692–1700. https://doi.org/10.1172/JCI20384.

Sakaue, H., Konishi, M., Ogawa, W., Asaki, T., Mori, T., Yamasaki, M., Takata, M., Ueno, H., Kato, S., Kasuga, M., Itoh, N., 2002. Requirement of fibroblast growth factor 10 in development of white adipose tissue. Genes Dev. 16, 908–912. https://doi.org/10.1101/gad.983202.

Sekine, K., Ohuchi, H., Fujiwara, M., Yamasaki, M., Yoshizawa, T., Sato, T., Yagishita, N., Matsui, D., Koga, Y., Itoh, N., Kato, S., 1999. Fgf10 is essential for limb and lung formation. Nat. Genet. 21, 138–141. https://doi.org/10.1038/5096.

Shimoaka, T., Ogasawara, T., Yonamine, A., Chikazu, D., Kawano, H., Nakamura, K., Itoh, N., Kawaguchi, H., 2002. Regulation of osteoblast, chondrocyte, and osteoclast functions by fibroblast growth factor (FGF)-18 in comparison with FGF-2 and FGF-10. J. Biol. Chem. 277, 7493–7500. https://doi.org/10.1074/jbc.M108653200.

Su, N., Jin, M., Chen, L., 2014. Role of FGF/FGFR signaling in skeletal development and homeostasis: learning from mouse models. Bone Res. 2, 14003. https://doi.org/10.1038/boneres.2014.3.

Terao, F., Takahashi, I., Mitani, H., Haruyama, N., Sasano, Y., Suzuki, O., Takano-Yamamoto, T., 2011. Fibroblast growth factor 10 regulates Meckel's cartilage formation during early mandibular morphogenesis in rats. Dev. Biol. 350, 337–347. https://doi.org/10.1016/j.ydbio.2010.11.029.

Wang, F., Kan, M., McKeehan, K., Jang, J.-H., Feng, S., McKeehan, W.L., 1997. A homeo-interaction sequence in the ectodomain of the fibroblast growth factor receptor. J. Biol. Chem. 272, 23887–23895. https://doi.org/10.1074/jbc.272.38.23887.

White, K.E., Cabral, J.M., Davis, S.I., Fishburn, T., Evans, W.E., Ichikawa, S., Fields, J., Yu, X., Shaw, N.J., McLellan, N.J., McKeown, C., FitzPatrick, D., Yu, K., Ornitz, D.M., Econs, M.J., 2005. Mutations that cause osteoglophonic dysplasia define novel roles for FGFR1 in bone elongation. Am. J. Hum. Genet. 76, 361–367. https://doi.org/10.1086/427956.

Wilkie, A.O.M., Morriss-Kay, G.M., 2001. Genetics of craniofacial development and malformation. Nat. Rev. Genet. 2, 458–468. https://doi.org/10.1038/35076601.

Yoshida, C.A., Yamamoto, H., Fujita, T., Furuichi, T., Ito, K., Inoue, K., Yamana, K., Zanma, A., Takada, K., Ito, Y., Komori, T., 2004. Runx2 and Runx3 are essential for

chondrocyte maturation, and Runx2 regulates limb growth through induction of Indian hedgehog. Genes Dev. 18, 952–963. https://doi.org/10.1101/gad.1174704.
Zhang, X., Ibrahimi, O.A., Olsen, S.K., Umemori, H., Mohammadi, M., Ornitz, D.M., 2006. Receptor specificity of the fibroblast growth factor family. J. Biol.Chem. 281, 15694–15700. https://doi.org/10.1074/jbc.M601252200.
Zheng, Q., Zhou, G., Morello, R., Chen, Y., Garcia-Rojas, X., Lee, B., 2003. Type X collagen gene regulation by Runx2 contributes directly to its hypertrophic chondrocyte–specific expression in vivo. J. Cell Biol. 162, 833–842. https://doi.org/10.1083/jcb.200211089.